International Journal for Multidisciplinary Research (IJFMR)
E-ISSN: 2582-2160 ● Website: www.ijfmr.com ● Email: editor@ijfmr.com

Powdered Cogon Grass (Imperata Cylindrica) as a Biosorbent for the Removal of Iron (II)

Aaron Lance R. Manalo[1], Fiona Daphne G. Gramata[2], Jamie Lee Ann S. Banzon[3], Mario Jose R. Sumalinog II[4]

[1,2,3]Undergraduate student, Department of Chemical Engineering, University of Santo Tomas
[4]MSnE Professor, Department of Chemical Engineering, University of Santo Tomas

Abstract

Iron (II) sulfate is a compound that is a waste byproduct in metal industries, contributing to excess iron levels present in water bodies. Iron (II) sulfate removal techniques include precipitation, filtration, and oxidation, which are effective but are more complex and costly. These techniques are largely affected by ion solubility, pH level of water, and the presence of other metal ions. Changes in pH can lead to the precipitation of other metal ions present and failure to filter properly may cause them to sediment and sink to the bottom. This research studied the potential of cogon grass (*Imperata cylindrica*) as a low-cost adsorbent for the removal of ferrous sulfate. Batch adsorption studies resulted in the adsorption capacity ranging around 200-350 mg/g, where increasing adsorbent dose correlated to an increase in percent removal but decrease in adsorption capacity. The percentage removal also increased with higher temperature, while the effect of agitation speed plateaued from 145 RPM above. The adsorption process conforms to pseudo-second-order kinetics with an R^2>0.96 and Freundlich isotherm model with R^2>0.97. FTIR analysis of cogongrass before and after $FeSO_4$ adsorption shows significant shifts in the IR spectrum, indicating new chemical bond formations, particularly with hydroxyl and carboxyl groups. Initially, peaks were identified for various functional groups like hydroxyls, alkanes, anhydrides, alkenes, and siloxanes. Post-adsorption, notable changes include the shifting and appearance of new peaks in hydroxyl, alkene, lignin, amine, and sulfonic acid bands, suggesting interactions with iron sulfate and the formation of organometallic complexes.

Keywords: adsorption, cogon grass, ferrous sulfate, iron

1. Introduction

Iron sulfate is a major component in industrial wastewater, particularly in metal industries such as steel and titanium dioxide production. The treatment of industrial wastewater containing iron sulfate reduces harmful levels of suspended solids, biochemical oxygen demand, and chemical oxygen demand [1]. However, the prolonged use of iron salts as a coagulant in wastewater treatment can lead to increased sludge production, posing heavy metal contamination in wastewater due to its chemical composition and toxic compounds [2,3]. The presence of dissolved ferrous sulfate in wastewater limits the effectiveness of conventional wastewater treatment such as sedimentation and filtration [4]. Adsorption involves the adherence of a solute to the surface of the adsorbent, which can be characterized by chemisorption, which forms chemical bonds, and physisorption, which relies on van der Waals forces [5,6].

Agricultural wastes have been studied as a promising material for water treatment using adsorption methods. Biomaterials, including agricultural waste, algae, bacteria, and industrial waste, are utilized as biosorbents for the process of heavy metal removal through biosorption [7]. Biosorption is often preferred in large-scale wastewater treatment due to its rapid adsorption kinetics, which offer low capital investment and operational cost. Furthermore, it can be performed under a wide range of pH, temperature, and the presence of other metal ions [8]. Biosorbents are primarily composed of functional groups such as hydroxyl, carboxyl, phenolic, and oxygen-containing groups, to which metal ions are bonded [9]. The functional groups in the biosorption process are influenced by adsorbent concentration, contact time, temperature, and the pH level [10]. The natural availability and abundance of biosorbent make them preferred for low-cost wastewater treatment [11]. Cogon grass *(Imperata cylindrica)* is perennial grass typically growing about 6-47 inches tall, making it an invasive species [12,13]. The chemical composition of cogon grass primarily consists of cellulose (51.61%); and holocellulose (77.69%) that is made up of cellulose, hemicellulose, and lignin (22%) [11]. The carboxyl and hydroxyl functional groups from hemicellulose and lignin, respectively, induce the ion exchange between heavy metal ions and protons from oxygen, resulting in an effective adsorption mechanism [14].

2. Literature Review

A study conducted towards the absorbency of cogon grass in various oil spill conditions revealed that cogon grass flowers adsorb much varying amounts of oil as compared to commercial oil absorbents, such as Peat Sorb. These results were attributed to the plants' hydrophobic nature, as well as its oil wettability. Additionally, even after 24 hours of simulating sea water ripple, among other conditions, said cogon grass samples were able to show good buoyancy, suggesting effectiveness in both land and water oil spills [15]. Another study of the removal of methylene blue (MB) used in dyes, food, and textile industries using cogon grass demonstrated a maximum removal of 99.09% and chemical oxygen demand reduction of 97.87%. This efficacy was observed through Fourier Transform Infrared Spectroscopy (FTIR) and Scanning Electron Microscopy (SEM) analysis, which revealed the development of new functional groups and a smoother surface of the leaves after adsorption due to the adhesion of dye particles [16].

The cadmium adsorption experiment with cogon grass involved granulating leaves to particle sizes of 78 µm to 100 µm, utilizing a cadmium nitrate tetrahydrate solution with a concentration of 1000 mg/L, and altering variables such as initial adsorbate concentration, contact time, and pH. It was found that equilibrium contact time depended on the initial concentration of the adsorbate and the size of the adsorbent, suggesting that adsorption is a surface phenomenon [17]. In copper and nickel adsorption experiments, base treatment was conducted on dried cogongrass particles to enhance nucleophilic sites for metal ion adsorption, with analysis revealing complexation and ion exchange mechanisms occurring between functional groups and metal ions, observed through shifts in FTIR and SEM-EDS peaks [18,19].

3. Methodology

The ferrous sulfate (99% purity) was obtained from University of Santo Tomas Laboratory Equipment and Supplies Office (UST LESO). Cogon grass was collected from the side of a rice field in Plaridel, Bulacan. The Proctor and Schwartz, Inc. Tray Dryer (60 cycles, 10 amperes), Thomas Wiley Mill Model 4, WS Tyler Sieve Shaker RX-29-16 (60 Hertz, 2.2 amperes), Biobase Shaking Water Bath SWB-B, Emerson Vacuum Pump C55JXHRL-4205 (0.5 HP, 1425/1725 RPM), Shimadzu Ultra-Violet Spectrometer UVmini-1240, and Agilent Cary 630 Fourier Transform Infrared Spectrophotometer used

for adsorbent and adsorbate preparation and experimentation were provided by the Chemical Engineering Laboratory of the University of Santo Tomas (UST) in Manila, Philippines.

3.1 Adsorbate and Adsorbent Preparation

0.0036M of ferrous sulfate stock solution was prepared by dissolving 1 g of ferrous sulfate in 1000 mL of distilled water. Cogon grass leaves were washed 3 times with distilled water to remove any impurities and sun dried for 3 days. The leaves were dried in a tray dryer at 80℃, ground and pulverized with a wiley mill prior to sieving at 150 µm - 250 µm. Afterwards, the cogongrass was re-washed then dried to remove leaching of contaminants.

3.2 Experimentation

Calibration curve. A series of known concentrations of ferrous sulfate solution was used and the peak wavelength of the solution was used as a basis to determine the molar extinction coefficient (ε). The molar extinction coefficient was used for future calculations where concentrations are unknown, then used for calculating the percentage removal.

Water bath shaker. All batch adsorption studies were conducted in 250mL erlenmeyer flasks placed inside a water bath shaker at 100 rpm and at a room temperature of 28℃, unless stated otherwise. To determine the effect of adsorbent dosage, 0.02 g, 0.04 g, 0.06 g, 0.08 g and 0.1 g of adsorbent were mixed with 100mL of the ferrous sulfate stock solution and shaken for approximately 60 min until equilibrium absorbance. To determine the effect of agitation speed (RPM), 0.02 g of adsorbent was mixed with 100 mL of ferrous sulfate stock solution and shaken at 100 RPM, 145 RPM, 190 RPM, 235 RPM, and 280 RPM. To determine the effect of temperature, 0.02 g of adsorbent was mixed with 100 mL of ferrous sulfate stock solution and shaken at 21℃, 24℃, 27℃, 30℃, and 33℃.

Vacuum filtration. A sample from the solution containing the adsorbate and adsorbent was collected for each trial after being shaken at 10 min intervals and the adsorbent was removed using vacuum filtration

Ultraviolet-Visible Spectroscopy. The Ultraviolet-Visible Spectroscopy (UV-Vis) was used to obtain the absorbance of the known ferrous sulfate solution and the change in concentration of the ferrous sulfate sample solution after adsorption.

3.3. Data Analysis

Determination of molar extinction coefficient. The initial concentrations of the ferrous sulfate samples and their corresponding absorbance values were plotted on the x-axis and y-axis, respectively, to produce the calibration curve from which the molar extinction coefficient (Ɛ) was determined. The molar extinction coefficient (Ɛ) was solved using the Beer-Lambert equation (1) where A is the absorbance, c (mol L^{-1}) is the concentration of the adsorbate in the solution, and l (cm) is the path length.

$$A = \varepsilon cl \quad (1)$$

Equilibrium curves. The absorbance of the ferrous sulfate sample after adsorption was plotted as a function of concentration. An equilibrium curve was constructed for each of the measured variables, specifically initial concentration, temperature, and agitation speed.

Kinetic models. Lagergren's pseudo-first-order (PFO) (2) and Ho's pseudo-second-order (PSO) (3) kinetic models were used to analyze the rate of adsorption iron in cogon grass. The amount of iron absorbed per time (q_t) in (mg g^{-1}) will be calculated using both equations where k_1 (h^{-1}) and k_2 (g mg^{-1} min^{-1}) is the rate constant of PFO and PSO, respectively.

$$ln(1-\frac{q_t}{q_e}) = -k_1 t \quad (2)$$

$$\frac{t}{q_t} = \frac{1}{k_2 {q_e}^2} + \frac{1}{q_e} t \quad (3)$$

Isotherm models. The linearized Langmuir isotherm equation (4) is used to characterize whether the adsorption in this study was homogeneous. The mechanism of adsorption was defined by the dimensionless separation factor (R_L) (5) where K_L is the Langmuir adsorption constant in (L mg^{-1}) and C_0 is the initial concentration of the adsorbate in the solution in (mg L^{-1}) and is favorable between 0 and 1.

$$\frac{Ce}{q_e} = \frac{1}{q_{max} K_L} + \frac{Ce}{q_{max}} \quad (4)$$

$$R_L = \frac{1}{1+K_L C_0} \quad (5)$$

The Freundlich isotherm equation (6) is used to determine if the adsorption behavior was heterogeneous at multiple layers through adsorption capacity (q_e) in (mg g^{-1}) where C_e in (mg L^{-1}) is the equilibrium concentration of the solute in the solution, K_F (mg g^{-1} x L $mg^{-1(1/n)}$) is the Freundlich adsorption constant, and n is the adsorption intensity. The value of 1/n is favorable between 0 and 1.

$$lnq_e = lnK_F + (\frac{1}{n}) lnCe \quad (6)$$

The linearized Temkin isotherm equation (7) assumes that the adsorption energy decreases linearly rather than logarithmically with an increase in the surface coverage where A_T relates to the maximum binding energy, while b_T is a constant related to the heat of adsorption.

$$q_e = \frac{RT}{b_T} ln(A_T) + \frac{RT}{b_T} ln(Ce) \quad (7)$$

The Sips isotherm equation (8) is a combination of Langmuir and Freundlich isotherm models and is ideal for complex adsorption involving monolayer and multilayer surfaces. The heterogeneity parameter (1/n) of this model will be useful to determine the dominant behavior of adsorption where m represents a homogeneous adsorption at a value close to 1 while a heterogeneous adsorption at a value close to 0, q_s (mg g^{-1}) is the saturation adsorption capacity, and K_S (mL/mg) is the Sips isotherm constant in equilibrium

$$q_e = \frac{q_s (K_s Ce)^m}{1+(K_s Ce)^m} \quad (8)$$

FTIR. Fourier Transform Infrared Spectroscopy (FTIR) was utilized to assess the chemical properties of cogongrass as an adsorbent before and after the adsorption process. The FTIR spectrometer was set up to record spectra from 4000 cm^{-1} to 500 cm^{-1}, ensuring detailed observation of functional group activity and bonding interactions.

4. Results and Discussion

4.1. Adsorption of Ferrous Sulfate at Varying Adsorbent Dosage

The data presented in Figure 4.1.1 represent the obtained adsorption capacity of the solutions with varying adsorbent dosage, following an interval of 10 mins per spectrophotometer measurement, respectively. Higher adsorbent dose correlates to a higher percentage removal while having a lower adsorption capacity.

Table 4.1.1. Adsorption Capacity at Varying Adsorbent Dosage

Trial	Contact Time (min)	Amount of Cogon Grass (g)	Percentage Removal (%)	Adsorption Capacity (mg/g)
1	60	0.02	73.593	361.961
2		0.04	86.196	206.488
3		0.06	88.597	146.661
4		0.08	98.199	122.749

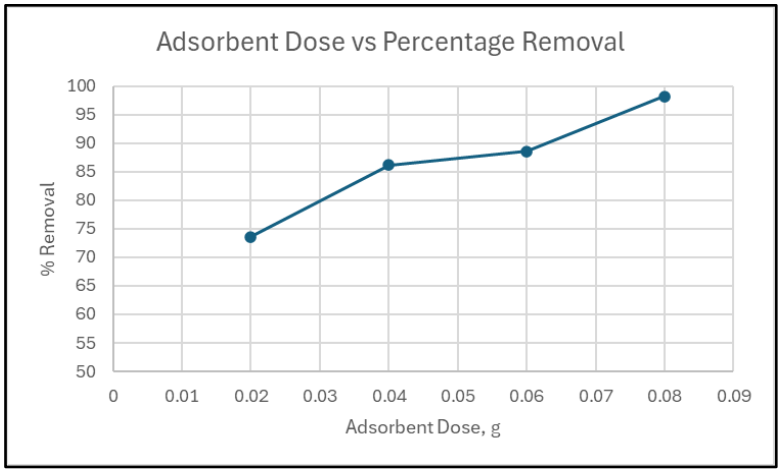

Figure 4.1.1. Percentage Removal of Cogon Grass at Varying Adsorbent Dose

Other researchers claim that while the total amount adsorbed by the adsorbent may increase, its capacity per adsorbent unit may decrease. A study regarding the adsorption of lead using Polypyrrole-Based Activated Carbon by Alghamdi et. al. claimed that higher doses of adsorbent may lead to aggregation, which decreases the available active sites for the adsorbent, therefore decreasing the efficiency of adsorption [20]. The general equilibrium time and adsorbent capacity of the experiment was found to be around 40-60 minutes and 200-350 mg/g respectively, which is similar to other biosorbents. A study based on using Chitosan as adsorbent for $FeSO_4$ yielded similar capacities, which were above 130 mg/g [22]. A raw blend of chitosan and starch also yielded similar results, which was around 200 mg/g [21] In terms of general biosorption, another research by Yang et. al determined that the biosorption capacity of Acid Black 172 and Congo red were 225.38 mg/g and 411.53 mg/g respectively [23]. Similarly, crab shells, from a study made by Vijayaraghavan et. al, demonstrated significant biosorption capacities of 243.9 mg/g for copper and 322.6 mg/g for cobalt [24] in a synthetic water sample. An adsorption study by Chyka et. al using activated charcoal at pH 4.5 and 7.5 yielded adsorption capacities of 102.96+/-4.49 mg/g and 100.94+/-19.02 mg/g respectively [25].

4.2. Adsorption of Ferrous Sulfate at Varying Temperature

Figure 4.2.1 and table 4.2.1 illustrate the percentage removal of $FeSO_4$ in relation to temperature. The trend of the data shows that higher temperatures correspond to a higher percentage removal.

Table 4.2.1. Adsorption Capacity at Varying Temperature

Trial	Temperature (Celsius)	Contact Time (min)	Percentage Removal (%)	Adsorption Capacity (mg/g)
1	21	40	63.214	316.070
2	24		67.812	339.061
3	27		70.440	352.199
4	30		71.754	358.768
5	33		73.067	365.337

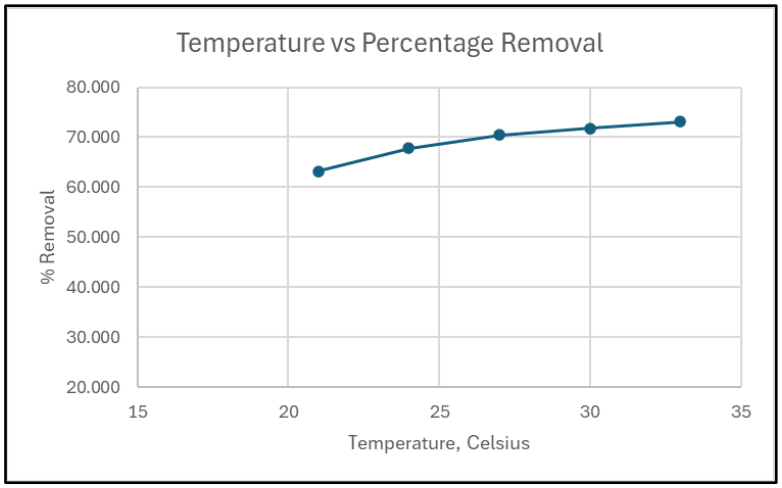

Figure 4.2.1. Percentage Removal of Cogongrass at Varying Temperature

The study of Aljar et al. on removal of Pb(II), Cd(II), Zn(II), and Co(II) from water using cellulose hydrogel beads identified more efficient adsorption as temperature is increased [26]. Another study by Budnyak et al. investigated chitosan deposited onto fumes silica surface for acid orange 8 dye capture, stating that an endothermic reaction is exhibited when adsorption capacity and temperature have a direct relationship, as depicted in Figure 4.2.1. Conversely, an exothermic reaction is observed when the adsorption capacity and temperature has an inverse relationship [27]. Budnyak et al., also examined the effect of temperature on endothermic reactions, where the mobility of the adsorbate molecules intensifies due to the increase of collision between adsorbent and adsorbate molecules, enhancing the accessibility of the active sites in the adsorbent surface at higher temperatures [28].

4.3. Adsorption of Ferrous Sulfate at Varying Agitation Speed

Figure 4.3.1 and Table 4.3.1 shows the summary of adsorption capacity and percent removal for the varying RPM experiments, where the corresponding absorbance and adsorption capacity for each sample within the experiment set were shown. All samples were set at increasing intervals of 45 RPM, taken off at equal periods, and checked within intervals of 5 minutes. It can be inferred that the effect of agitation speed is only illustrated from 100-145 RPM. Subsequent data sets do not differentiate well enough to establish a trend.

Table 4.3.1. Adsorption Capacity at Varying Agitation Speed

Trial	Agitation Speed (RPM)	Contact Time (min)	Percentage Removal (%)	Adsorption Capacity (mg/g)
1	100	50	71.097	355.484
2	145		78.323	391.613
3	190		78.979	385.044
4	235		79.636	398.182
5	280		79.636	398.182

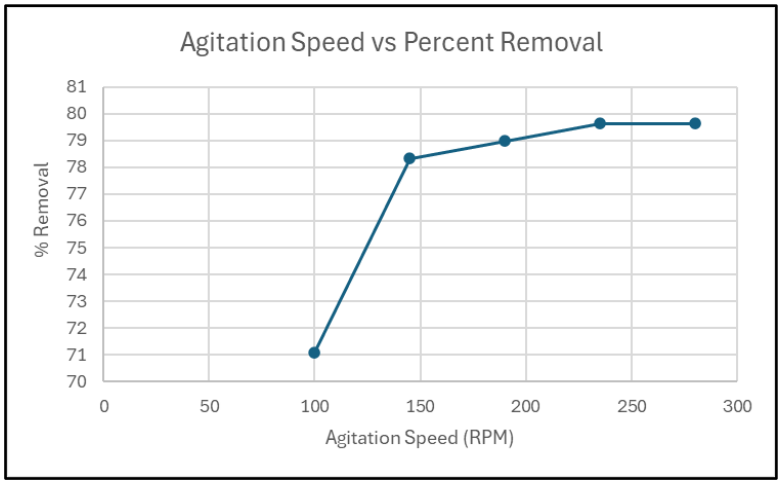

Figure 4.3.1. Percentage Removal of Cogon Grass at Varying Agitation Speed

Similarly, other studies also suggest that while increasing the RPM can enhance the adsorption process by improving mixing and contact efficiency between adsorbate and adsorbent, there is a point beyond which further increases in RPM do not lead to proportional gains in adsorption efficiency. The earlier study mentioned that uses of activated carbon derived from polypyrrole for the adsorption of lead ions also found that once optimal agitation conditions were found, increased RPM did not significantly enhance lead removal efficiency. This plateau effect suggests that there are optimal agitation speeds that maximize adsorption efficiency without the need for higher energy input, which aligns with the general observation in adsorption kinetics that beyond a certain agitation level, the gains in adsorption efficiency become minimal [20].

4.4. Fourier Transform Infrared Spectroscopy (FTIR) Analysis

FTIR analysis of cogongrass before and after adsorption with FeSO4 reveals significant peak shifts, indicating the formation of new chemical bonds between the ferrous sulfate and functional groups in the cogongrass such as hydroxyl and carboxyl groups. The shifts to longer or shorter wavelengths are dictated by changes in the molecular mass and vibration energy of atoms within the molecule, affecting the IR absorption spectrum. Before adsorption, the cogongrass showed a range of functional group signatures: hydroxyl groups at 3600-3200 cm^{-1}, C-H alkane stretching at 2917-2850 cm^{-1}, conjugated anhydride at 1732 cm^{-1}, and C-C stretching indicating alkenes at 1617 cm^{-1}. Additional bands were noted for lignin, C-

O alkyl aryl ether and amine stretching, and Si-O-Si asymmetric stretching in siloxanes, demonstrating the complex molecular makeup of cogongrass [29, 30, 31, 32].

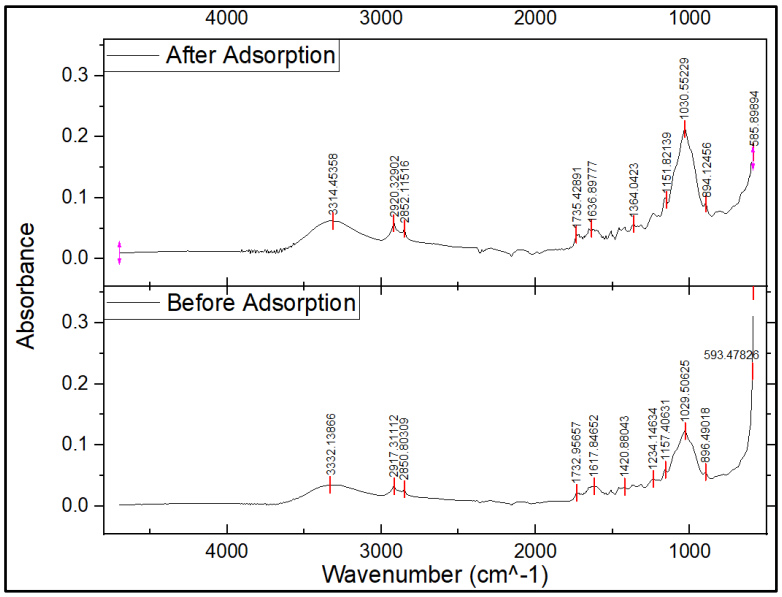

Figure 4.4.1. FTIR Spectra of Cogon Grass Before and After Adsorption

After $FeSO_4$ adsorption, the IR spectra of cogongrass shifted: the hydroxyl peak moved from 3316 to 3329 cm^{-1}, indicating hydrogen bonding interactions with hydrated Fe^{2+} ions. Peaks related to C-H stretching remained within the alkane region, while new peaks and shifts indicated interactions with iron sulfate, such as a shift to 1735 cm^{-1} and a new peak at 1636 cm^{-1} for alkenes. Changes in lignin were suggested by disturbances at 1364 cm^{-1}, and shifts in amine and sulfonic acids bonds were seen at 1240 and 1151 cm^{-1}, respectively. The presence of sulfate ions was confirmed by a new peak at 1033 cm^{-1}, and other structural changes indicative of organometallic complex formations were observed at lower spectral regions, aligning with shifts typically seen around 500 cm^{-1} in similar adsorption studies [33, 34, 35, 36].

4.5. Comparison to Kinetic Models

Adsorption kinetics were analyzed using the pseudo-first-order and pseudo-second-order models, represented by linearized equations shown in Equations 2 and 3 in Section 3. The kinetics data were summarized in table 4.5.1, as well as shown individually in figures 4.5.1 and 4.5.2. Only one model fitted well with the data; the pseudo-second-order model showed higher correlation coefficients (R^2 values of 0.9603, 0.9808, 0.9851, and 0.9987 for adsorbent doses of 0.02g, 0.04g, 0.06g, 0.1g respectively) than the pseudo-first-order model (R^2 values of 0.1082, 0.3828, 0.4151, 0.4227). This indicates that the adsorption process aligns more closely with pseudo-second-order kinetics.

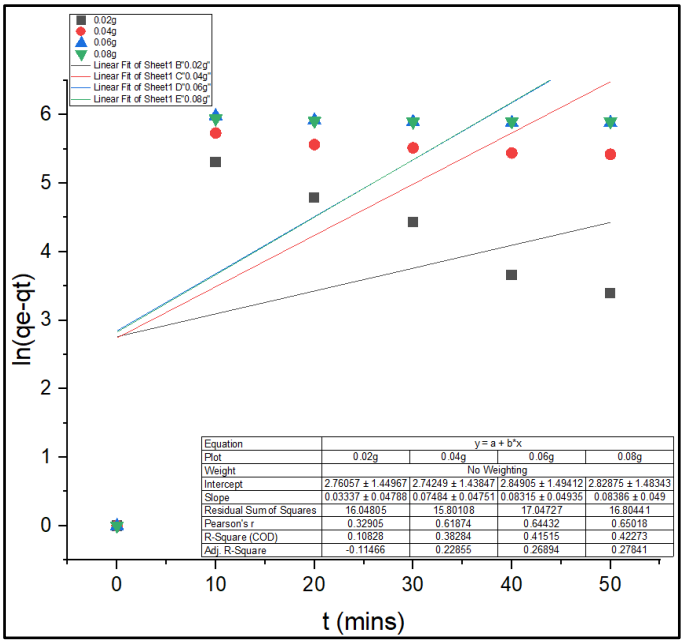

Figure 4.5.1. t vs ln(qe-qt) Plot, Pseudo-First-Order Kinetic Model

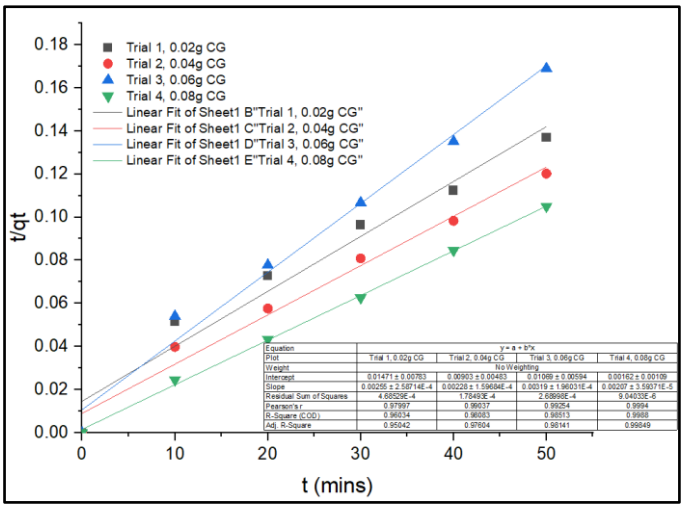

Figure 4.5.2. t vs ln(qe-qt) Plot, Pseudo-Second-Order Kinetic Model

4.6. Comparison to Adsorption Isotherms

Figure 4.6.1 to 4.6.4 show the resulting plot between Langmuir, Freundlich, Sips, and Temkin isotherms respectively. Based on the following coefficients of determination (0.8571, 0.9716, 0.7500, 0.8749), it is shown that the adsorption interactions follow the Freundlich model most closely. The R_L parameter on the Langmuir model shows a value of 0.00059, which indicates a favorable adsorption. Similarly, the Freundlich model exhibits a 1/n value of 0.5471, which also indicates favorable adsorption. This indicates that the surface of the adsorbent can be considered heterogeneous, where differences in the activation energy in any specific site can determine the likelihood of it being reacted upon.

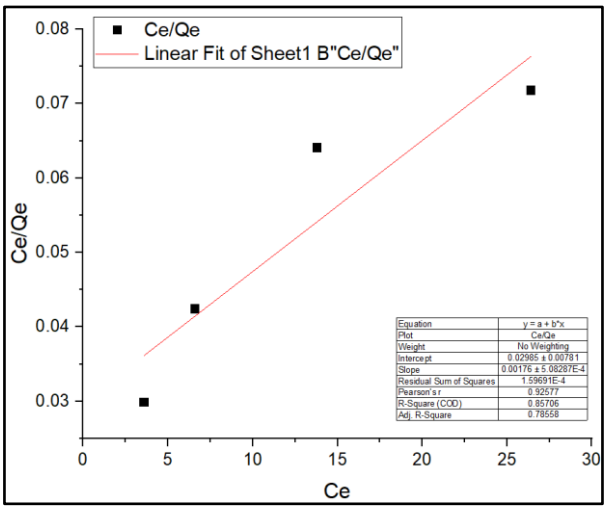

Figure 4.6.1. Ce vs Ce/Qe, Langmuir Isotherm Model

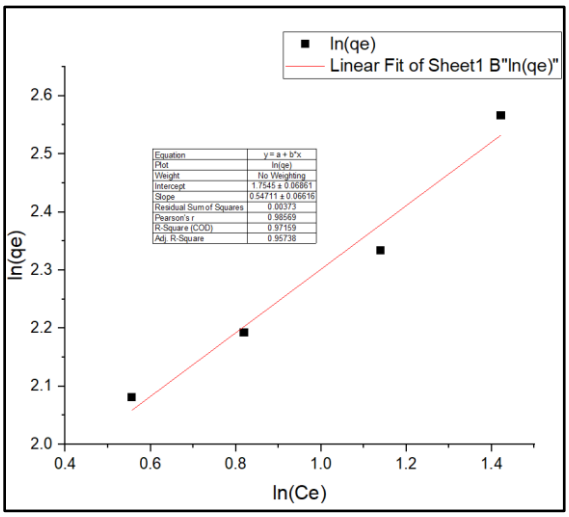

Figure 4.6.2. ln(Ce) vs ln(qe), Freundlich Isotherm Model

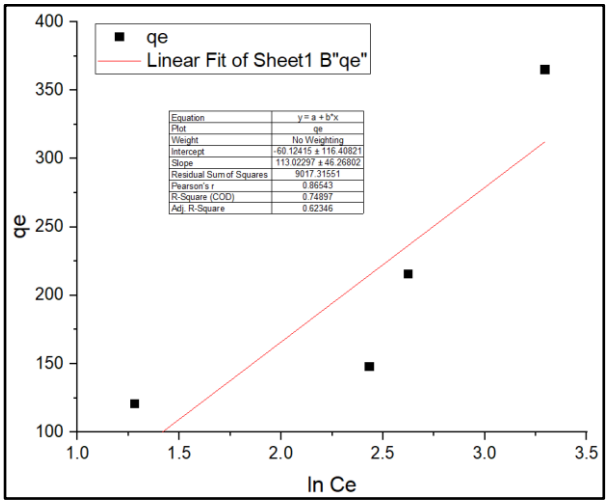

Figure 4.6.3. ln(Ce) vs qe, Temkin Isotherm Model

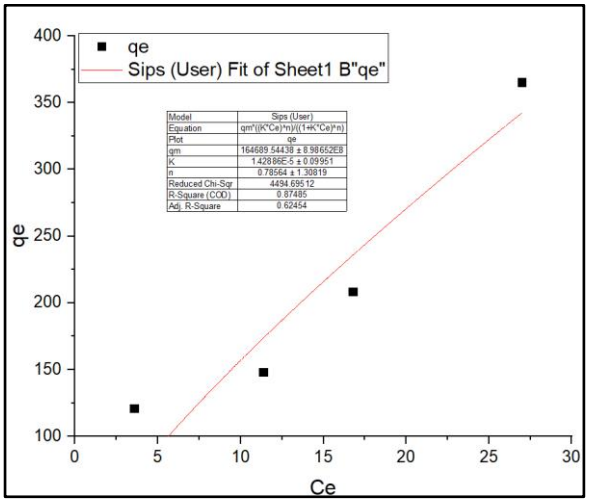

Figure 4.6.4. Ce vs qe, Sips Isotherm Model

This result is similar to the study by researchers who investigated the phosphate adsorption capacity of lanthanum-modified bentonite, which was characterized using the Freundlich isotherm model to reflect the heterogeneous nature of the adsorption sites [37]. Their findings demonstrated that the modification of bentonite with lanthanum significantly enhances its adsorption efficiency, primarily due to the increased surface area and the addition of more functional sites capable of chemically binding phosphate ions. The adsorption capacity observed peaked at a certain concentration, indicative of surface site saturation where no further phosphate ions could be adsorbed despite an increase in their concentration [38].

5. Conclusion and Recommendations

5.1 Conclusion

Cogon grass has proven to be an effective adsorbent for removing iron (II) from a synthetic water setting, exhibiting adsorption capacities (200-350 mg/g) and removal efficiencies (60%-99%) comparable to other

known water contaminant adsorbents. This is comparable to other adsorption capacities regarding $FeSO_4$, such as chitosan adsorbent (124.78-132.04 mg/g), starch-chitosan biopolymer blend (61-115 mg/g), and activated charcoal (102-100.94 mg/g) at pH 4.5 and 7.5. It conforms to typical biosorbent behavior in kinetic and isotherm models, favoring the Ho's Pseudo-Second-Order kinetic model over Lagrangen's Pseudo-First-Order, as evidenced by determination coefficients ranging from 0.96 to 0.99 versus 0.1 to 0.4, respectively. The Freundlich isotherm model, which suggests heterogeneous adsorption sites, fits the adsorption data best with an R^2 value of 0.97, indicating variable activation energies for adsorption at different sites compared to other models like Langmuir, Sips, and Temkin.

The temperature of the solution enhances the adsorption rate, potentially due to lower activation energy requirements, although the overall adsorbent capacity remains unaffected by temperature changes. Agitation speed impacts adsorption efficiency only up to a certain point (145 RPM), beyond which increased speed does not further influence the process. FTIR analysis identifies functional groups, particularly hydroxyl and carbonyl, that facilitate the binding of ferrous sulfate to cogongrass, a process similar to other studies involving $FeSO_4$. These groups, along with cogongrass's inherent cellulose and lignin content indicate the biomass's utility in adsorbing heavy metals effectively.

5.2 Recommendations

For future research, several recommendations are proposed based on the findings from the study on cogongrass-$FeSO_4$ adsorption. First, further exploration of a thermodynamic study, including the creation of a Van't Hoff plot, determining the Gibbs energy, and enthalpy of reaction will deepen understanding of the process' feasibility and energetic efficiency. Comparatively, investigating chemically-treated adsorbents could reveal enhancements in adsorption capacity due to increased functional groups, such as hydroxyl groups, which facilitate more effective heavy metal removal [39]. Additionally, the application of Response Surface Methodology (RSM) is recommended to optimize the adsorption process by developing mathematical models that correlate various operational parameters with adsorption efficiency. Lastly, employing Scanning Electron Microscopy and Energy Dispersive Spectroscopy (SEM-EDS) will provide detailed insights into the adsorbent's surface morphology and elemental composition, helping to visualize the mechanisms underlying adsorption [40].

Appendix

Table 1. Adsorption Capacity Data at Varying Adsorbent Dosage

Trial	Amount of Cogon Grass (g)	Contact Time (min)	Percentage Removal (%)	Adsorption Capacity (mg/g)
1	0.02	0	0	0
		10	38.783	193.914
		20	54.987	274.937
		30	62.189	310.947
		40	71.192	355.960
		50	73.593	367.963
		60	72.392	361.961
		0	0.000	0

2	0.04	10	50.186	125.465
		20	69.391	173.479
		30	74.193	185.482
		40	81.395	203.487
		50	86.196	215.490
		60	82.595	206.488
3	0.06	0	0	0
		10	66.391	110.651
		20	80.795	134.658
		30	85.596	142.660
		40	88.597	147.661
		50	88.597	147.661
4	0.08	0	0	0
		10	81.395	101.743
		20	92.198	115.247
		30	95.799	119.749
		40	94.598	118.248
		50	95.199	118.998
		60	98.199	122.749

Table 2. Adsorption Capacity Data at Varying Water Bath Temperature

Trial	Temperature (°C)	Contact Time (min)	Percentage Removal (%)	Adsorption Capacity (mg/g)
1	21	0	0	0
		5	25.771	128.856
		10	30.369	151.847
		15	49.419	247.096
		20	46.792	233.959
		25	53.361	266.803
		30	56.645	283.226
		35	59.930	299.648
		40	63.214	316.070
2	24	0	0	0
		5	30.369	151.847
		10	33.654	168.269
		15	42.850	214.252
		20	49.419	247.096
		25	57.302	286.510
		30	57.302	286.510
		35	63.214	316.070
		40	67.812	339.061
3	27	0	0	0
		5	29.056	145.278
		10	34.968	174.838
		15	43.507	217.536
		20	50.733	253.665
		25	55.988	279.941

		30	58.616	293.079
		35	63.871	319.355
		40	70.440	352.199
4	30	0	0	0
		5	32.340	161.700
		10	34.968	174.838
		15	46.792	233.959
		20	54.018	270.088
		25	61.900	309.501
		30	63.214	316.070
		35	66.498	332.492
		40	71.754	358.768
5	33	0	0	0
		5	30.369	151.847
		10	38.252	191.261
		15	44.164	220.821
		20	55.331	276.657
		25	63.871	319.355
		30	66.498	332.492
		35	69.126	345.630
		40	73.067	365.337

Table 3. Adsorption Capacity Data at Varying Agitation speed

Trial	Agitation speed (RPM)	Contact Time (min)	Percentage Removal (%)	Adsorption Capacity (mg/g)
1	100	0	0	0
		5	30.369	151.847
		10	32.997	164.985
		15	46.792	233.959
		20	50.733	253.665
		25	54.674	273.372
		30	58.616	293.079
		35	65.185	325.924
		40	68.469	342.346
2	145	0	0	0
		5	42.850	214.252
		10	59.930	299.648
		15	73.067	365.337
		20	77.009	385.044
		25	76.352	381.759
		30	77.666	388.328
		35	77.009	385.044
		40	75.695	378.475
3	190	0	0	0
		5	46.792	233.959
		10	63.214	316.070
		15	71.754	358.768
		20	77.666	388.328
		25	75.695	378.475
		30	77.009	385.044
		35	78.323	391.613
		40	78.979	394.897

4	235	0	0	0
		5	47.449	237.243
		10	61.243	306.217
		15	74.381	371.906
		20	79.636	398.182
		25	77.666	388.328
		30	77.666	388.328
		35	78.323	391.613
		40	77.009	385.044
5	280	0	0	0.000
		5	44.164	220.821
		10	61.243	306.217
		15	73.067	365.337
		20	77.009	385.044
		25	78.979	394.897
		30	78.979	394.897
		35	77.666	388.328
		40	78.323	391.613

Acknowledgement

We, the researchers, would like to express our heartfelt gratitude to the following people who contributed to the completion of this thesis:

Our dedicated thesis adviser, **Engr. Mario Jose R. Sumalinog II, MSEnE.**, whose support and guidance have been remarkably useful throughout this research journey. His expertise, patience, accessibility, and encouragement have been the foundation in developing the framework of this study.

Engr. Divine Angela Sumalinog, PhD, whose effort have been integral for the successful arrangement of our laboratory schedule, granting us permission to use laboratory equipment and facilities needed for our experimentation.

The ChE laboratory Technicians, **Sir Oliver and Sir Wendell**, whose assistance have been essential for the proper use of the laboratory equipment and for overcoming equipment-related difficulties.

To our **professors**, whose professionalism in their respective fields has been helpful in understanding essential concepts and processes related in our study.

To our **friends**, whose valuable insights have ignited new ideas crucial for the proper execution of our experiments, and whose companionship has made our thesis experiments more manageable.

To our **family and parents**, whose constant love, support, and effort in acquiring necessary materials, along with their financial support, ensured seamless experimentation.

References

1. Ng WJ. Industrial Wastewater Treatment [Internet]. Google Books. World Scientific; 2006 [cited 2024 May 1]. Available from: https://books.google.com.ph/books?hl=en&lr=&id=DM42DwAAQBAJ&oi=fnd&pg=PR5&dq=industrial+wastewater+treatment&ots=E08Zu1CLDc&sig=iGdIKD-ZTy2zcyT33ET0loTsj2s&redir_esc=y#v=onepage&q=industrial%20wastewater%20treatment&f=false
2. Wu Z, Ji S, Li YY, Liu J. A review of iron use and recycling in municipal wastewater treatment plants and a novel applicable integrated process. Bioresource Technology. 2023 Jul 1;379:129037–7.

3. Santos MT, Lopes PA. Sludge recovery from industrial wastewater treatment. Sustainable Chemistry and Pharmacy. 2022 Oct;29:100803.
4. U.S. Environmental Protection Agency. Drinking Water Contaminants – Standards and Regulations [Internet]. Washington, DC: U.S. EPA; [updated 2017 Jan 19; cited 2024 May 2]. Available from: https://19january2017snapshot.epa.gov/dwstandardsregulations
5. Pillai SB. Adsorption in Water and Used Water Purification. Handbook of Water and Used Water Purification. 2020;1–22.
6. Deng F, Luo XB, Ding L, Luo SL. Application of Nanomaterials and Nanotechnology in the Reutilization of Metal Ion From Wastewater. Nanomaterials for the Removal of Pollutants and Resource Reutilization. 2019;149–78.
7. Adewuyi A. Chemically Modified Biosorbents and Their Role in the Removal of Emerging Pharmaceutical Waste in the Water System. Water. 2020 May 29;12(6):1551.
8. Gouda SA, Taha A. Biosorption of Heavy Metals as a New Alternative Method for Wastewater Treatment: A Review. Egyptian Journal of Aquatic Biology and Fisheries [Internet]. 2023 Mar 1 [cited 2023 May 23];27(2):135–53. Available from: https://ejabf.journals.ekb.eg/article_291671.html
9. Adewuyi A. Chemically Modified Biosorbents and Their Role in the Removal of Emerging Pharmaceutical Waste in the Water System. Water. 2020 May 29;12(6):1551.
10. Michalak I, Chojnacka K, Witek-Krowiak A. State of the Art for the Biosorption Process—a Review. Applied Biochemistry and Biotechnology [Internet]. 2013 Jul 1 [cited 2020 May 9];170(6):1389–416. Available from: https://www.ncbi.nlm.nih.gov/pmc/articles/PMC3696181/
11. Ibrahim S, Baharuddin SNIB, Ariffin B, Hanafiah MAKM, Kantasamy N. Cogon Grass for Oil Sorption: Characterization and Sorption Studies. Key Engineering Materials. 2018 Aug;775:359–64.
12. Bryson CT, Carter R. Cogongrass,Imperata cylindrica, in the United States. Weed Technology. 1993 Dec;7(4):1005–9.
13. Maddox V, Bryson C, Byrd J. Cogongrass [Imperata cylindrica (L.) Beauv.] [Internet]. 2018. Available from: https://www.researchgate.net/publication/327940710_Cogongrass_Imperata_cylindrica_L_Beauv
14. Yu, H., Wang, J., Yu, J., Chi, R. (2020, December). Adsorption performance and stability of the modified straws and their extracts of cellulose, lignin, and hemicellulose for Pb2+: pH effect. Arabian Journal of Chemistry, 13(12), 9019-9033. https://doi.org/https://doi.org/10.1016/j.arabjc.2020.10.024
15. Wiloso EI, Barlianti V, Anggraini IF, Hendarsyah H. POTENTIAL OF COGON GRASS AS AN OIL SORBENT. Jurnal Kimia Terapan Indonesia [Internet]. 2012 Jun 1 [cited 2023 Apr 22];14(1). Available from: https://inajac.lipi.go.id/index.php/InaJAC/article/view/121
16. Su CXH, Teng TT, Alkarkhi AFM, Low LW. Imperata cylindrica (Cogongrass) as an Adsorbent for Methylene Blue Dye Removal: Process Optimization. Water, Air, & Soil Pollution. 2014 Apr 18;225(5).
17. Kamal A, Zu M, Zakaria HM, Shariff Che Ibrahim. Adsorption of Cd(II) Ions from Aqueous Solutions by Lalang (Imperata cylindrica) Leaf Powder: Effect of Physicochemical Environment. Journal of Applied Sciences. 2007 Feb 15;
18. Hanafiah MAKM, Zakaria H, Wan Ngah WS. Preparation, Characterization, and Adsorption Behavior of Cu(II) Ions onto Alkali-Treated Weed (Imperata cylindrica) Leaf Powder. Water, Air, and Soil Pollution. 2008 Nov 30;201(1-4):43–53.

19. Hanafiah MAKM, Zakaria H, Ngah WSW. Base Treated Cogon Grass (Imperata cylindrica) as an Adsorbent for the Removal of Ni(II): Kinetic, Isothermal and Fixed-bed Column Studies. CLEAN - Soil, Air, Water. 2010 Mar 22;38(3):248–56.
20. Alghamdi AA, Al-Odayni AB, Saeed WS, Al-Kahtani A, Alharthi FA, Aouak T. Efficient Adsorption of Lead (II) from Aqueous Phase Solutions Using Polypyrrole-Based Activated Carbon. Materials (Basel). 2019 Jun 24;12(12):2020. doi: 10.3390/ma12122020. PMID: 31238508; PMCID: PMC6630235.
21. Boughanmi R, Steinbach C, Gerlach N, Oelmann M, Beutner C, Schwarz S. Ecological Sorption of Iron and Sulfate Ions onto Starch and Chitosan Biopolymer Blend. Polysaccharides. 2023; 4(3):325-342. https://doi.org/10.3390/polysaccharides4030019
22. Chyka PA, Butler AY, Herman MI. Ferrous sulfate adsorption by activated charcoal. Vet Hum Toxicol. 2001 Feb;43(1):11-3. PMID: 11205069.
23. Yang Y, Wang G, Wang B, Li Z, Jia X, Zhou Q, et al. Biosorption of Acid Black 172 and Congo Red from aqueous solution by nonviable Penicillium YW 01: Kinetic study, equilibrium isotherm and artificial neural network modeling. Bioresource Technology. 2011 Jan;102(2):828–34.
24. Janek Weißpflog, Regine Boldt, Benjamin Kohn, Ulrich Scheler, Dieter Jehnichen, Václav Tyrpekl, Simona Schwarz,Investigation of mechanisms for simultaneous adsorption of iron and sulfate ions onto chitosan with formation of orthorhombic structures,Colloids and Surfaces A: Physicochemical and Engineering Aspects,Volume 592,2020,124575,ISSN 0927-7757,https://doi.org/10.1016/j.colsurfa.2020.124575.
25. Biosorption of copper(II) and cobalt(II) from aqueous solutions by crab shell particles. Bioresource Technology [Internet]. 2006 Aug 1;97(12):1411–9. Available from: https://www.sciencedirect.com/science/article/abs/pii/S096085240500324X
26. Aljar MAA, Rashdan S, Almutawah A, El-Fattah AA. Synthesis and Characterization of Biodegradable Poly(vinyl alcohol)-Chitosan/Cellulose Hydrogel Beads for Efficient Removal of Pb(II), Cd(II), Zn(II), and Co(II) from Water [Internet]. ResearchGate. 2023. Available from: https://www.researchgate.net/publication/370018062_Synthesis_and_Characterization_of_Biodegradable_Polyvinyl_alcohol-ChitosanCellulose_Hydrogel_Beads_for_Efficient_Removal_of_PbII_CdII_ZnII_and_CoII_from_Water
27. Budnyak TM, Błachnio M, Slabon A, Jaworski A, Tertykh VA, Deryło-Marczewska A, et al. Chitosan Deposited onto Fumed Silica Surface as Sustainable Hybrid Biosorbent for Acid Orange 8 Dye Capture: Effect of Temperature in Adsorption Equilibrium and Kinetics. Journal of physical chemistry C/Journal of physical chemistry C [Internet]. 2020 Jun 16 [cited 2024 Apr 29];124(28):15312–23. Available from: https://www.ncbi.nlm.nih.gov/pmc/articles/PMC7493206/
28. Khalid FE, Ahmad SA, Zakaria NN, Shaharuddin NA, Sabri S, Azmi AA, et al. Application of Cogon Grass (Imperata cylindrica) as Biosorbent in Diesel-Filter System for Oil Spill Removal. Agronomy [Internet]. 2021 Nov 1;11(11):2273. Available from: https://www.mdpi.com/2073-4395/11/11/2273/htm
29. Invasive Plants: Cogongrass - UF/IFAS Extension: Solutions for Your Life [Internet]. sfyl.ifas.ufl.edu. [cited 2024 May 6]. Available from: https://sfyl.ifas.ufl.edu/archive/hot_topics/environment/cogongrass.shtml

30. Bunmai, K., Osakoo, N., Deekamwong, K., Rongchapo, W., Keawkumay, C., Chanlek, N., Prayoonpokarach, S., & Wittayakun, J. (2017). Extraction of silica from cogon grass and utilization for synthesis of zeolite NaY by conventional and microwave-assisted hydrothermal methods. Journal of The Taiwan Institute of Chemical Engineers, 83, 152-158.
31. Nandiyanto ABD, Oktiani R, Ragadhita R. How to Read and Interpret FTIR Spectroscope of Organic Material. Indonesian Journal of Science and Technology [Internet]. 2019 Mar 7;4(1):97. Available from: https://ejournal.upi.edu/index.php/ijost/article/download/15806/pdf
32. Lee CM, Kubicki JD, Fan B, Zhong L, Jarvis MC, Kim SH. Hydrogen-Bonding Network and OH Stretch Vibration of Cellulose: Comparison of Computational Modeling with Polarized IR and SFG Spectra. The Journal of Physical Chemistry B. 2015 Nov 30;119(49):15138–49.
33. Marta CU, Măluțan T, Clovica S. Iron gall inks influence on papers' thermal degradation FTIR spectroscopy applications [Internet]. ResearchGate. 2009. Available from: https://www.researchgate.net/publication/282724424_Iron_gall_inks_influence_on_papers%27_thermal_degradation_FTIR_spectroscopy_applications
34. Vitanesa, Lora & Purba, Radja & Lesbani, Aldes & Said, Muhammad. (2017). Bentonite intercalated organometallic complex as adsorbent of procion red. Science & Technology Indonesia. 1. 9-16. 10.26554/sti.2017.2.1.9-16.
35. Ali Q, Ali S, El-Esawi MA, Rizwan M, Azeem M, Hussain AI, Perveen R, El-Sheikh MA, Alyemeni MN, Wijaya L. Foliar spray of Fe-Asp confers better drought tolerance in sunflower as compared with FeSO4: Yield traits, osmotic adjustment, and antioxidative defense mechanisms. Biomolecules. 2020;10(9):1217. doi:10.3390/biom10091217.
36. Reitzel K, Andersen FØ, Jensen HS, et al. Phosphate adsorption by lanthanum modified bentonite clay
37. Mo J, Li Q, Sun X, Zhang H, Xing M, Dong B, Zhu H. Capacity and Mechanisms of Phosphate
38. Younas F, Mustafa A, Farooqi ZUR, Wang X, Younas S, Mohy-Ud-Din W, et al. Current and Emerging Adsorbent Technologies for Wastewater Treatment: Trends, Limitations, and Environmental Implications. Water [Internet]. 2021 Jan 1;13(2):215. Available from: https://www.mdpi.com/2073-4441/13/2/215/htm
39. Myers, R. H., Montgomery, D. C., & Anderson-Cook, C. M. (2016). Response surface methodology: process and product optimization using designed experiments. John Wiley & Sons.
40. Sen, K., & Chattoraj, S. (2021). A comprehensive review of glyphosate adsorption with factors influencing mechanism: Kinetics, isotherms, thermodynamics study. In Intelligent Environmental Data Monitoring for Pollution Management (pp. 93–125). https://doi.org/10.1016/b978-0-12-819671-7.00005-1